Assessment of Solar Variability Through the Analysis of TSI Observations Recorded by the FY3E/JTSIM/DARA Radiometer

J.-P. Montillet[1], W. Finsterle[1], P. Zhu[2,3], M. Haberreiter[1], S. Koller[1], D. Pfiffner[1], D. Wu [2], X. Ye[2], D. Yang[2], W. Fang[2], J. Qi[2], P. Zhang[2]

[1]Physikalisch-Meteorologisches Observatorium Davos/World Radiation Center (PMOD/WRC), Davos, Switzerland
[2]CIOMP, CAS, Dongnan Hu Road 3888, Changchun, 100190, Jilin, China
[3]Institute for Advanced Study, Shenzhen University, Shenzhen, China

Key Points:

- Time-frequency analysis of the the total solar irradiance (TSI) dataset recoreded by the FY3E/JTSIM/DARA
- DARA observations closest to the TIM/TSIS measurements in terms of mean value comparison (0.07 W/m^2)
- Analysis of the integration of the new JTSIM-DARA dataset into the 43 year long TSI composite time series

Corresponding author: J.P. Montillet, jean-philippe.montillet@pmodwrc.ch

Abstract

Since the late 1970s, successive satellite missions have been monitoring solar activity and recording Total Solar Irradiance (TSI) data. The Digital Absolute Radiometer (DARA) on board the Chinese FY3E spacecraft was launched on July 4, 2021, and has since been recording TSI observations. Here, we analyze these observations and demonstrate their sensitivity to significant variations in temperature within the radiometer's cavities. Additionally, we observed minimal degradation (5 ppm) in the recorded observations after 2 years in orbit, resulting from exposure to ultraviolet and extreme ultraviolet radiation. Comparing the new dataset's mean values with observations from active instruments on other spacecraft (i.e., PMO6 on board the VIRGO/SOHO and the TIM/TSIS), along with the Solar Irradiance Absolute Radiometer (SIAR) also on board FY3E/JTSIM, we find that DARA observations closely align with TIM/TSIS, with a difference of approximately 0.07 W/m^2. Based on these findings, we generate a new TSI dataset at a 6-hour sampling interval. Finally, we have incorporated this new dataset into the TSI composite time series released by the PMOD/WRC. The results indicate that the inclusion of DARA-recorded observations does not alter the consistency, reliability, and stability of the time series, particularly when examining variations during the last four solar minima.

1 Introduction

Total Solar Irradiance (TSI) stands as a critical parameter for comprehending and predicting Earth's climate system, exerting a pivotal role in establishing the planet's energy balance through both incoming and outgoing electromagnetic radiation. TSI is defined as the integrated solar energy flux across its entire spectrum reaching the top of the atmosphere at the mean Sun-Earth distance of 1 AU (the astronomical unit). The reliable and continuous monitoring of TSI's absolute value is indispensable for understanding, reconstructing, and forecasting Earth's climate. However, accurately measuring TSI has been a challenging task, requiring the deployment of radiometers on spacecraft recording continuously observations since the late 1970s. Various publications have extensively discussed the TSI data records, contributing to our understanding of this important parameter. Studies, e.g., Kopp et al. (2005), Thuillier et al. (2006), Kopp and Lean (2011) or Yeo et al. (2014), have analyzed TSI measurements recorded from overlapping missions over the past 43 years.

To further advance TSI monitoring capabilities, the Joint Total Solar Irradiance Monitor (JTSIM) has been developed as the next-generation instrument for long-term TSI monitoring in space. This instrument, built by the Changchun Institute of Optics, Fine Mechanics and Physics Chinese Academy of Sciences (CIOMP/CAS) in Changchun, China, is embedded into the Chinese Fengyun-3E spacecraft. The Fengyun program, supported by the National Satellite Meteorological Center (NSMC) of China, aims to develop a series of Chinese meteorological spacecraft. The JTSIM comprises the Digital Absolute Radiometer (DARA) from the PMOD/WRC in Davos, Switzerland, and the Solar Irradiance Absolute Radiometer (SIAR) from CIOMP/CAS. These two radiometers are mounted on the same pointing system to measure TSI accurately. DARA is the latest type of radiometers developed by the PMOD/WRC (Davos, Switzerland), featuring several innovations compared to the previous generation. SIAR, on the other hand, employs an electrically calibrated differential heat-flux transducer with a cavity for efficient radiation absorption (Wang et al., 2007; Zhu et al., 2023).

Here, we evaluate the TSI measurements recorded by DARA. Song et al. (2021), Montillet et al. (2022) or Zhu et al. (2023) have already discussed the radiometer's features (e.g., cavity, aperture size), the pre-flight calibration of the first light and the data reduction from raw observations to level 1. Overall, DARA has three (cavity radiometers) electrical substitution radiometers (channel A, channel B, and channel C, also called

cavity A, B or C). The (active) cavities are alternately shielded and exposed to the sun by periodically activating the shutter. Cavity B is the nominal cavity operating at a one minute rate. Cavity C is one of the backup cavity operating once every 10 days, whereas cavity A is the other backup cavity operating irregularly and used as the reference cavity when checking the housekeeping data (e.g., voltage, current). The cavities are aligned in a triangle which differs from older versions developed at PMOD such as the PMO6 radiometer on board of the VIRGO/SOHO mission. The new design has multiple advantages, e.g. reduction of stray light, and the so-called non-equivalence effect (Montillet et al., 2022; Zhu et al., 2023). The operating rate is important to estimate the exposure time to UV/EUV radiation and modelling the degradation of the material (e.g., the coating paint inside the cavity). Here, we focuses on the next level product and the time-frequency analysis of the TSI time series from the first light to the end of July 2023. The observed solar features are compared with other TSI products recorded by other active missions (i.e. VIRGO/SOHO or TIM/TSIS).

Moreover, we include the new product into the so-called TSI composite time series, incorporating all the observations available recorded by successive space instruments spanning 4 decades. As all satellite observations are limited in time, constructing composites is a key aspect to the investigation of TSI fluctuations over several decades. Merging all these observations is a difficult exercise with both a scientific and a statistical challenge (Dudok de Wit et al., 2017). Various algorithms have produced the TSI composite time series either without (Wilson, 1997; Fröhlich & Lean, 2004; Mekaoui & Dewitte, 2008) or with modelling the stochastic noise properties Dudok de Wit et al. (2017); Montillet et al. (2022). A comprehensive discussion of the robustness of these various methodologies is out of the scope of the presented work. Readers can refer to Dudok de Wit et al. (2017); Scafetta and Willson (2019); Montillet et al. (2022); Amdur and Huybers (2023). Here, we compare the TSI composite time series including the new DARA product using the algorithm developed by Montillet et al. (2022) with other available datasets.

The next section is an overview of the various past and currently active radiometers on board of spacecrafts together with the released TSI datasets. The Section 3 focuses on the new TSI products at various data rates (i.e., minute, 6-hourly and daily) and the comparison with TSI observations recorded by some currently active radiometers. We perform a time-frequency statistical analysis in order to understand the various noise backgrounds (i.e. solar noise, instrumental artifacts) influencing the data. We also discuss the influence of the degradation of the radiometer due to long exposure to UV/EUV light. The last section, Section 4, is the integration of the DARA TSI product (daily rate) within the TSI composite time series.

2 Description of the TSI missions over the past 43 years

Table 1 displays the instruments and the processing centers providing the observations relative to the various missions past and present. The data processing, including corrections for all a priori known influences such as the distance from the sun (normalized to 1 AU), radial velocity of the sun, and thermal, optical, and electrical corrections, are usually implemented by each processing center, leading to level 1 data. Most of these instruments observe on a daily basis, with occasional interruptions and outliers. Usually, one to three of them operate simultaneously, although some days are devoid of observations. Note that *PMODv21a* (also called *PMO6v8*) is the new VIRGO/SOHO dataset released in March 2021 by PMOD using a new software described in Finsterle et al. (2021). *PREMOS (v1)* is the released version described in Schmutz et al. (2013). ERBE/ERBS and HF/NIMBUS-7 ERB datasets are retrieved from the PMOD archive and the corrections made by C. Fröhlich, which are explained in Fröhlich (2006).

We have not included the previous test missions using a similar radiometer as the FY3E/JTSIM/SIAR on board of FY3A/B/C satellites. For a comprehensive overview,

Mission/Experiment/Instrument	Version	Start Date	End Date
HF/NIMBUS-7 ERB	-	11/1978	1/1993
ERBE/ERBS	-	10/1984	8/2003
VIRGO/SOHO	PMODv21a	01/1996	active
PREMOS/PICARD	v1	06/2010	03/2014
ACRIM1/SMM	1	2/1980	7/1989
ACRIM2/UARS	7/14	10/1991	9/2000
ACRIM3/ACRIMSAT	11/13	04/2000	11/2013
TIM/SORCE	19	02/2003	02/2020
TIM/TCTE	4	12/2013	05/2019
TIM/TSIS	3	11/01/2018	active
NORSAT/CLARA	1	07/2017	active
FY3E/JTSIM/DARA	1	07/2021	active
FY3E/JTSIM/SIAR	1	07/2021	active

Table 1: Overview of the datasets used in this study including the start and end dates for each mission and the latest version released by the various centers.

the reader can refer to Qi et al. (2015) and Zhu et al. (2023). Note that *active* in Table 1 means that the instrument is still operating.

3 Data Analysis

This section focuses mostly on the time-frequency analysis of the observations recorded by the DARA and some comparisons with other TSI products at different rates (i.e. daily, 6-hourly). We also discuss the sensitivity of the recorded TSI observations to instrumental noises (e.g., cavity temperature). The second subsection is the analysis of the ratio between the nominal cavity and the back-up cavity (i.e. early increase, degradation).

3.1 Time-Frequency Analysis

Zhu et al. (2023) have evaluated the first light on August 18 2021 (01h 22min UTC) for DARA at 1361.99 $\pm$0.05 W/m^2 for cavity B. The cavity A recorded the first TSI value at 1361.36 $\pm$0.12 W/m^2 at 13h 12 min UTC and 1361.85 $\pm$0.05 W/m^2 on cavity C at 04h 56min UTC. Figure 1 shows the recorded TSI observations for channel B (blue), C (green) and A (red). The time series displays a good consistency without many outliers. Note that the large drop in the TSI on the 20th of April 2023 is due to the total solar eclipse (Young et al., 2023). Other large TSI excursions are identified as outliers due to the off-pointing of the radiometer (e.g., deep space measurements). To further check the integrity of the DARA observations, we perform a frequency analysis displayed in Figure 2. From previous studies, e.g., Andersen et al. (1994), Fröhlich et al. (1997) or Montillet et al. (2022), the PSD can be divided in various areas to analyse the solar noise. Solar noise results from photospheric activity associated with granules varying at different timescales

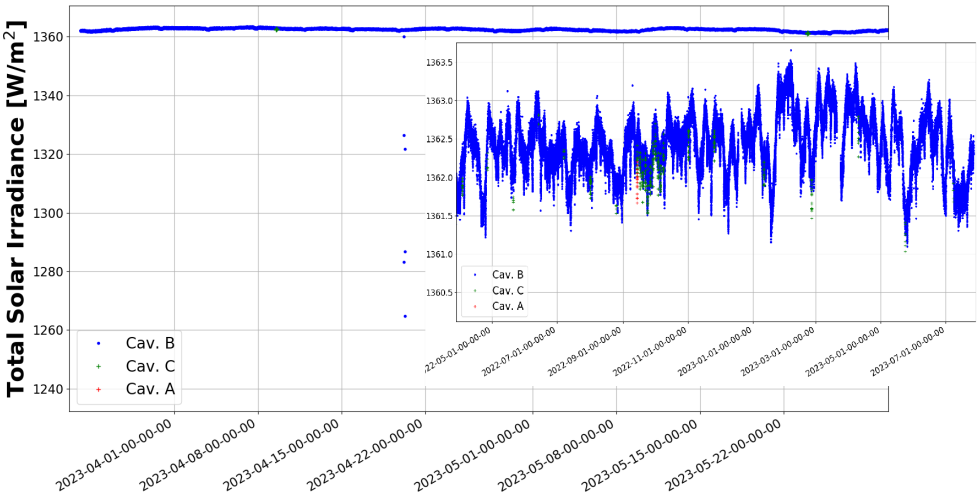

Figure 1: TSI observations recorded by the DARA from the various cavities: channel B (blue), channel C (green) and A (purple). The channel B operates at 1 min. rate, C at 10 day rate, and A irregularly acting as reference cavity. For convenience, we have inserted a zoom of the time series (on a short period).

over a few hours (e.g., sunspots) to a decade (e.g., solar cycle), which generate fluctuations in the recorded irradiance values (Shapiro et al., 2017).

In the minute rate TSI time series, we look at two frequency bands: G1 at [1-100] days and G2 at [1-30] minutes. The G1 frequency group is generally associated with the solar activity with events varying over days or longer (Fröhlich et al., 1997; Dudok de Wit et al., 2017; Shapiro et al., 2017; Montillet et al., 2022). The vertical dotted lines (black) F1, F2 and F3 are associated with the frequencies at 27, 9 and 7 days respectively which corresponds to the various modes of the solar rotation. The quasi 27-day solar cycle is caused by the sun's differential rotation (presumably first observed by Galileo Galilei or Christoph Scheiner in the first half of the 17th century - (von Savigny et al., 2019)). We can also observe in Figure 2 that a spike at 101 minutes for the satellite orbital revolution (yellow dashed vertical line) can be seen only in the PSD of the observations recorded by the SIAR. The SIAR data have been filtered by the CIOMP team, therefore the recording rate is approximately 10 min. We can see the impact of applying several band-pass filters in the trend and noise of the PSD.

Below the 1 Hz/day, we observe the photospheric activity associated with P-modes (around 5 min.), granulation (around [6, 16] minutes), meso-granulation (around [16, 166] minutes) and granulation (up to 1 day) (Andersen et al., 1994; Fröhlich et al., 1997). This solar activity generates fluctuations in TSI at different timescales. Shapiro et al. (2017) discuss also the various instrumental noises at high frequencies (below 5 min.) which is difficult to dissociate from the solar noise. In the G2 frequency band (below 1 h), the DARA frequency spectrum is not completely flat showing some modulations. The SIAR frequency spectrum displays four large spikes (i.e. 20 min, 26 min, 34 min and 51 min). The first and second frequency spikes may be associated with the recording window (20 to 26 min) of the instrument.

To investigate further the various spikes and frequency modulations, one needs to take into account the features of the JTSIM platform on which both DARA and SIAR

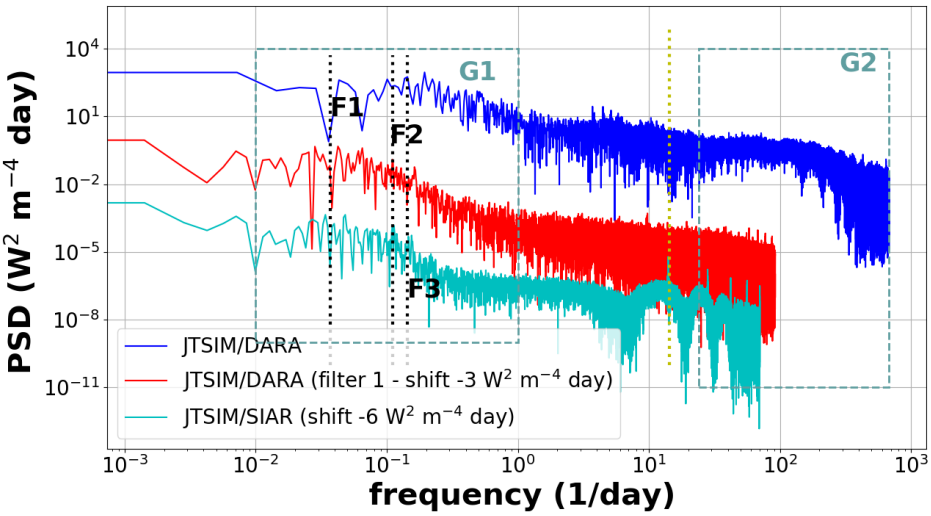

Figure 2: Power spectrum analysis of the DARA 1 min rate TSI time series using the Welch's method: raw level 2 observations (blue), applying filter 1 (red) and SIAR (cyan). We emphasize the two frequency bands G1 at [1-100] days and G2 at [1-60] minutes. The black vertical dotted lines correspond to 27 (F1), 9 (F2) and 7 days (F3). The yellow dashed vertical line is the line at the frequency of the satellite revolution (101 minutes).

instruments are mounted. The platform rotates every 4 days to perform the Deep Space (DS) measurements which were only used during the commission phase (post-launch) in order to evaluate mainly the DS corrections (Song et al., 2021; Zhu et al., 2023). During these measurements, the cavity exchanges radiation with a different thermal background in the shutter-open case, where the cavity radiates to deep space, compared to the closed case where the cavity's thermal emission is reflected by the (gold-coated) backside of the shutter. The DS correction is then required to compensate the thermal background effect which is linked with the geometry of the cavity and the electronics of the instruments (Walter et al., 2020; Song et al., 2021). In addition, the platform movement is hard-coded in the spacecraft software system and can be neither interrupted nor overwritten. During this maneuver, the cavity temperature variations look like a seesaw dropping between 4K and 10K over a 14h period. In the appendices, Figure A1 and A2 display the cavity temperature with an emphasis on the large excursions. In addition, due to the polar orbit of the spacecraft, the transition from night to day also induces temperature variations of $\sim$ 7K. Therefore, the variability in the cavity temperature disturbs the nominal setup of the instrument and thus degrading the quality of the recorded TSI measurements.

In order to show this sensitivity, we apply a filter, also called filter 1 in the remainder of this study, using the cavity temperature to detect the large variations and identify the corresponding measurements. To filter the excursions of the recorded temperature, we use a threshold adjusted over time varying between 272K and 287K. The selected temperatures are displayed in red in Figure A1 and A2 with small variations of less than 2K. Figure 3 displays the results of applying this filter. The included zoom emphasizes a pattern in the TSI observations: every 4 days the measurements have a large scatter. This period corresponds to the regular DS measurements. We can remove all the observations acquired in the DS mode. These measurements increase the scatter of the time series. However, they do not contribute to the TSI fluctuations originating from solar activity, e.g. sunspot blocking, intensification due to bright faculae, and other el-

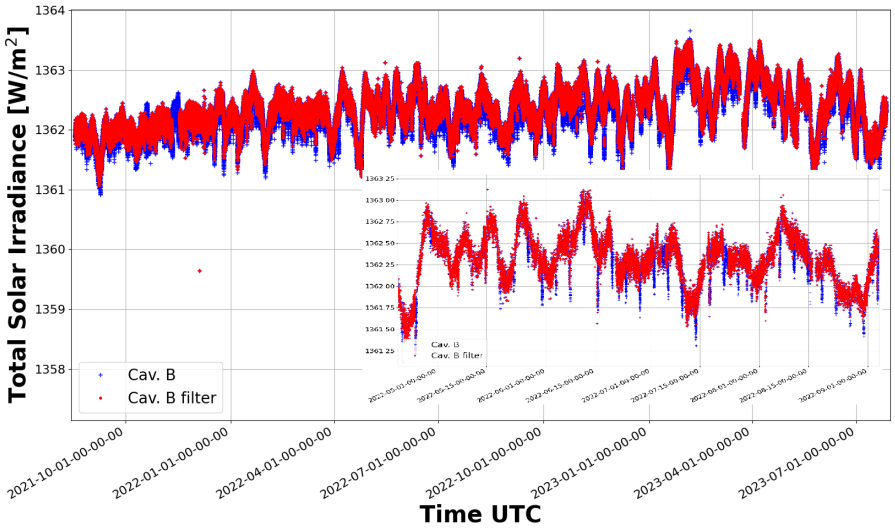

Figure 3: DARA TSI observations after applying the filter based on the cavity temperature (filt. 1). We display the channel B before (blue) and after filtering (red). Note that for conveniences, we display the full time series between 1357 W/m^2 and 1364 W/m^2 and a zoom on a selected period.

ements. They should be classify as instrumental noise a fortiori. The rate of the filtered times series is then reduced to virtually 7.8 min due to the high number of removed observations. Figure A3 shows the PSD of the TSI observations recorded by the VIRGO/PM06 radiometer with an emphasis on the P-modes. Previous works (Andersen et al., 1994; Fröhlich et al., 1997) demonstrate that in the granulation, the meso-granulation and supergranulation no activity can be detected in the VIRGO/PMO6 spectrum. The spectrum decreases in a power-law of approximately f^{-2}. Figure A3 displays the power-law model and supports this assumption. Comparing with the PSD of the filtered DARA observations, the slope is similar. we may then assume that similar stochastic processes are present.

Furthermore, we observe many small amplitude spikes ranging around 16 min, 18 min, 21 min and 25 min. They may correspond to the recording window (20 -26 min) of the instrument. Some of them are common between DARA and SIAR spectrum due to the similar operating time. As discussed before, there is a slight shift between these frequencies due to the filtering of the SIAR observations. Note that the frequencies at 16 min and 18 min can be further eliminated if we filter more observations with a tighter criteria on selecting the cavity temperature variations (e.g., below 1K).

Figure A4 and A5 display the PSD of the 6-hourly rate with and without filtering of the DARA observations. One can notice in the non-filtered data some spikes ranging from 4 days to 13 hours (i.e. [4, 2, 1.33, 1, 0.82, 0.68, 0.57, 0.5] days). All these frequencies are related to the DS measurements and the resulting sensitivity to the large variations of the cavity temperature. In fact, the first harmonic of the DS measurement is 4 days, the second harmonic is 2 days, the third one is 1.33 days, the fourth one is 1 day. The frequency of the spikes matches all the harmonics up to the 8th order. After filtering, we can see that all these frequencies disappear (see green spectrum). The slopes of the spectrum associated wit the various instruments are similar which means that similar stochastic noise processes (i.e. coloured and white noises) are contained in the ob-

servations, supporting our previous result about the spectrum of the raw DARA observations. In particular, the SIAR and DARA frequency spectra (with or without filtering) correlate together very well in the low frequency (see before the F3 dotted line - at 7 days). The frequency spectrum of the TIM/TSIS and the DARA (or the SIAR) seem to be shifted of approximately 1.83 days. This frequency shift may be explained by the large number of missing observations in the TIM/TSIS product which is supported by the lower rate (8.35h) compared with the SIAR (6.01h) or the DARA (6.10h (unfiltered), 6.52h (filtered)) products. Note that the spectrum of the VIRGO/PMO6 is only here for reference. We use the hourly product released by PMOD/WRC (Finsterle et al., 2021).

Moreover, Figure A6 shows the PSD of the TSI observations recorded by the various instruments for the daily sampling rate. The DARA frequency spectrum is similar to VIRGO/PMO6 and TIM/TSIS when using filter 1. For the unfiltered data, there are two spikes at 2 and 4 days which correspond to the DS measurements (i.e. first and second harmonic) as discussed previously.

Now, Table 2 presents the statistics computed on the observations recorded by the DARA, VIRGO/PMO6, TIM/TSIS, and SIAR at various sampling rates (i.e., minute, 6-hourly, and daily). In general, the mean value of VIRGO/PMO6 is lower than the estimates of the DARA and SIAR. The statistics associated with the SIAR observations are larger than the DARA ones across all sampling rates. DARA closely aligns with TIM/TSIS (within a margin of less than 0.07 W/(m^2)). The SIAR records values above TIM/TSIS by approximately 0.26 W/(m^2). Both DARA and SIAR observations are on average larger than the ones associated with the VIRGO/PMO6 observations.

Mission/Experiment/Instrument	Minute		(6-)Hourly		Daily	
TSI level ($\mu \pm \sigma$ [W/m^2])	μ	σ	μ	σ	μ	σ
VIRGO/PMO6	1361.10	0.52	1361.24(*)	0.38	1361.24	0.37
TIM/TSIS (+)	-	-	1362.32	0.38	1362.32	0.39
FY3E/JTSIM/DARA	1362.31	1.36	1362.32	0.41	1362.30	0.56
FY3E/JTSIM/DARA (filt. 1)	1362.35	0.37	1362.34	0.36	1362.35	0.36
FY3E/JTSIM/SIAR	1362.58	0.69	1362.58	0.45	1362.58	0.43
FY3E/JTSIM/DARA [DC]	1362.31	1.35	1362.32	0.41	1362.30	0.56
FY3E/JTSIM/DARA (filt. 1 [DC])	1362.35	0.37	1362.35	0.36	1361.35	0.36

Table 2: Statistics - mean (μ) $\pm$ Uncertainties (σ) in W/m^2 - for various active missions estimated for the period 18 August 2021 - 27 July 2023 . (*) means that we use the hourly product for VIRGO/PMO6. The sampling rate of the TIM/TSIS observations is only available in 6-hourly and daily products. The last two rows are the degradation-corrected TSI observations (see *[DC]*).

3.2 Degradation-Correction

The degradation of radiometers on board of satellites due to UV/EUV radiation has been a topic of research for the last 3 decades. Several approaches to deal with degradation-correction have been proposed (Fröhlich, 2003, 2006). Each of the data sets listed in Table 1 consist of the TSI measurements from an active (continuously operated) and at least one back-up (occasionally operated) channel. To assess instrument degradation, scien-

tists compare the measurements from the active channel with those from the occasionally operated backup channel(s). The specific procedure for this assessment varies and is often determined by the instrument team, evolving over the course of the experiment's lifetime. Correction of degradation is particularly important when comparing and/or combining the TSI measurements from different missions into a single composite time series as discussed in the next section. Various algorithms have been proposed, based on different assumptions and often using personal judgement when processing the data sets (Fröhlich, 2006; Dewitte & Nevens, 2016; Wilson, 2014). Finsterle et al. (2021) have recently developed an algorithm based on machine learning and data fusion to process the TSI observations without filtering or applying any sort of data pre-processing which can be assimilated to "human refinement". This algorithm is based on three basic assumptions i/ the degradation curve is a function of the exposure time. The exposure time is the time when the instrument (in space) observes the sun; ii/ there is no degradation at the time of the first measurement taken in space; iii/ the degradation function is a smooth monotonic decreasing curve. The latter assumption involves that there is no additional source of degradation of the TSI measurements starting during the mission life time. The algorithm is currently employed to correct the TSI observations recorded by the VIRGO/PMO6 radiometer. Here, we apply this algorithm to correct any degradation which could have degraded observations recorded by the nominal cavity of the DARA.

Figure A7 displays the estimated degradation in channel B. The estimation is done using the ratio of the measurements recorded by the two channels as a function of the mission days. The ML algorithm fits an isotonic function similar to the correction of the channel A of the VIRGO/PMO6 radiometer. When looking at the ratio, there is no early increase phenomenon that was previously documented in the analysing the observations recorded by VIRGO/PMO6 (Finsterle et al., 2021) and PREMOS/PMO6 data (Schmutz et al., 2013; Ball et al., 2016). The change of coating paint used in the DARA's cavity may explain this result. Also, our analysis have shown that the frequent deep space measurements have a negative impact on the stability of the time series. Therefore, we cannot exclude that the early increase phenomenon which should last less than 10 exposure days (e.g., 5 exposure days for the VIRGO/PMO6 (Finsterle et al., 2021)) could be somehow masked by the temperature instability of the cavity. Moreover, we can see that the degradation does not start before mission days 680 (66 days of exposure time). That is the time needed for the saturation of the coating paint before starting the degradation of its absorption properties. This topic is comprehensively investigated in Remesal Oliva (2021). Overall, the correction is very small of around 0.5 ppm for a period covering 25 months within the scatter of the observations of around $\pm$ 200 ppm. Therefore, we conclude that no degradation can be observed on the recorded measurements.

Finally, we compare the statistics of the degradation-corrected TSI time series in Table 2 with the raw observations (i.e. between the upper and lower part of the table). The results show that the difference at any recording rate is marginal (below 0.01 W/m^2). This outcome is anticipated as a result of the minor adjustment of the TSI observations.

4 TSI Composite Including the JTSIM-DARA Product

Previously, we have introduced the TSI composite time series gathering all the TSI data recorded by satellite missions since the late 1970s. In our effort to assess the integration of the DARA daily rate dataset into this time series, we conduct a time-frequency analysis similar to the approach adopted by Dudok de Wit et al. (2017) and Montillet et al. (2022). The algorithm employed to generate the TSI composite, developed by Montillet et al. (2022), is based on the former PMOD/WRC TSI composite released by Fröhlich (2006). Consequently, the product resulting from Montillet et al. (2022) is also regarded as the replacement of the discontinued product updated by Fröhlich (2006).

The previous time series released by Dudok de Wit et al. (2017), Fröhlich (2006) and Montillet et al. (2022) are called respectively *Composite 1 (C1)*, *Composite 2 (C2)* and *Composite 3 (C3)* in the following text. The product when including the daily DARA product is called *Composite 4 (C4)*, and with the SIAR product *Composite 5 (C5)*. *Composite 6 (C6)* is the latest TSI time series published by Dewitte and Nevens (2016) and updated by Dewitte et al. (2022). The DARA daily rate time series is the so-called FY3E/JTSIM/DARA filt. 1 in Table 2. Moreover, C1 is the TSI community consensus composite, the benchmark against which any new results must be compared.

We perform a comparative analysis of the new composite time series by examining the differences in solar minima. The results are presented in Table 3. It is worth noting that the period used for averaging the solar minima are the same ones selected in Dudok de Wit et al. (2017) and Montillet et al. (2022). Our findings indicate variations among the C1, C2, C3 and C6 consistent with the observations discussed in Montillet et al. (2022), where the methodology for constructing the TSI composite time series accounts for the differences in solar minima across various solar cycles. For example, the fluctuations of the solar minima between Solar Cycle 21/22 and 22/23 ($\Delta I_{22/23-21/22}$) do not agree between the composites. The difference is positive for the C1, whereas it is negative or null for the other composites. This disagreement has been discussed in Montillet et al. (2022), and it is due to the processing methodology of the TSI observations for the first missions (e.g., HF/NIMBUS-7 ERB, ERBE/ERBS). The fluctuation between the other solar cycles (i.e Solar Cycle 22/23, 23/24, 24/25) is more homogeneous in terms of the sign value (i.e. negative for all of them). As previously said, readers interested specifically in the making of the TSI composites can refer to the literature (Fröhlich, 2006; Dudok de Wit et al., 2017; Dewitte et al., 2022; Montillet et al., 2022). Our main result is that C3, C4 and C5 do not show many differences at the level of the solar minima (i.e. below 0.01 W/m^2). Thus, the inclusion of the DARA or the SIAR observations has no influence on the TSI composite. The difference between two successive solar minima (e.g., $\Delta I_{22/23-21/22}$) can help detect a (global) trend following the methodology used in Dudok de Wit et al. (2017) and Montillet et al. (2022). The results show that these differences are marginal, with associated uncertainties large enough (i.e. at least twice the mean value) to discredit any assumptions on the trend. Any visual effects or short-term trends are most likely related to the coloured noise rather than a physical phenomenon generated by the sun's activity, corroborating previous discussions (Dudok de Wit & Kopp, 2020) and supporting recent analysis (Schmutz, 2021; Montillet et al., 2022; Amdur & Huybers, 2023). Finally, Figure A8 shows the TSI composite time series C3 and C4. Figure A9 displays the frequency spectrum comparing C1, C2, and C4. The frequency analysis shows that the power spectrum are very similar which means that they all contain similar stochastic noise at a similar amplitude. Last, the difference between C3 and C4 is displayed in Figure A10. 90 % of the points are between the $/pm$ 0.01 W/m^2. The mean value is approximately 0.0001 W/m^2 with an uncertainty of 0.008 W/m^2, therefore the inclusion of the JTSIM-DARAv1 product does not change the characteristics of the TSI composite at level of 0.01 W/m^2.

5 Conclusions

This work focuses on a comprehensive analysis of TSI observations recorded by the DARA instrument onboard the FY3E spacecraft. The study encompasses various sampling rates, i.e. minute, hourly, and daily data, and includes comparisons with other active radiometers (i.e. VIRGO/PMO6 and TIM/TSIS) together with the SIAR which is also mounted on the same platform as the DARA.

Our findings shed light on several key aspects of the TSI observations. Notably, we demonstrate the sensitivity of the recorded TSI to DS measurements, driven by significant variations in the cavity temperature. In contrast, the SIAR observations proves resilient to such sensitivity due to the (effective) control of cavity temperature, which

TSI level ($\mu \pm \sigma$ [W/m^2])		Composite Name											
		C1		C2		C3		C4		C5		C6	
		μ	σ	μ	σ	μ	σ	μ	σ	μ	σ	μ	σ
Solar Cycle 21/22	*Minimum* (SM_1)	1360.51	0.13	1360.59	0.12	1360.59	0.13	1360.59	0.13	1360.59	0.13	1360.53	0.11
	$\Delta I_{21/22-20/21}$	-	-	-	-	-	-	-	-	-	-	-	-
Solar Cycle 22/23	*Minimum* (SM_2)	1360.69	0.14	1360.57	0.15	1360.59	0.13	1360.59	0.13	1360.59	0.13	1360.51	0.12
	$\Delta I_{22/23-21/22}$	**0.18**	**0.27**	**-0.02**	**0.27**	**0.0**	**0.26**	**0.0**	**0.26**	**0.0**	**0.26**	**-0.02**	**0.23**
Solar Cycle 23/24	*Minimum* (SM_3)	1360.53	0.04	1360.42	0.06	1360.41	0.04	1360.41	0.04	1360.41	0.04	1360.47	0.04
	$\Delta I_{23/24-22/23}$	**-0.17**	**0.18**	**-0.15**	**0.21**	**-0.18**	**0.17**	**-0.18**	**0.17**	**-0.18**	**0.17**	**-0.05**	**0.16**
Solar Cycle 24/25	*Minimum* (SM_4)	-	-	-	-	1360.37	0.07	1360.37	0.07	1360.37	0.07	1360.49	0.06
	$\Delta I_{24/25-23/24}$	-	-	-	-	**-0.04**	**0.11**	**-0.04**	**0.11**	**-0.04**	**0.11**	**-0.02**	**0.21**

Table 3: Estimation of TSI at solar minimum (*Minimum*) over the last 43 years from TSI time series (mean μ and standard deviation σ) released by Dudok de Wit et al. (2017) (*C1*), by Fröhlich (2006) (*C2*), by Montillet et al. (2022) *Composite 3 (C3)* and by Dewitte and Nevens (2016) (*C6*). The new TSI composite including the daily JTSIM-DARAv1 product and the daily sampling of the SIAR observations are abbreviated to (*C4*) and (*C5*). The difference in irradiance between solar minima (*SM*) from consecutive solar cycles (e.g., $\Delta I_{22/23-21/22}$) is also displayed with the uncertainties (bold text)

minimizes large excursions. Note that we have accessed only the filtered SIAR data for this study. Our work also delves into an evaluation of degradation caused by exposure to UV/EUV radiations in space, employing the algorithm developed by Finsterle et al. (2021). The results show only marginal degradation after 2 years following the spacecraft launch. We also find that DARA observations are at a level close to TIM/TSIS records with a difference of the mean value less than 0.07 W/m^2. Note that the mean value of the SIAR measurements is above, with a mean value difference of 0.26 W/m^2. Based on these results, we make the 6-hourly rate product, which underwent filtration based on cavity temperature (referred to as DARA filt. 1) and corrected for degradation. This product, denoted as JTSIM-DARAv1, is now available to the public.

Finally, JTSIM-DARAv1 has been inserted in the TSI composite time series using the algorithm developed by Montillet et al. (2022). The TSI composite gathers all the TSI observations recorded since the late 1970s. A comparison with the TSI composite released regularly by PMOD/WRC (Montillet et al., 2023) showcases only marginal differences (i.e. below 0.01 W/m^2). This result demonstrates the overall consistency and reliability of including the JTSIM-DARAv1 product into the composite. Looking forward, the TSI composite time series releases by the PMOD team will consistently includes the JTSIM-DARAv1 product, ensuring a robust and continuous record for the benefit of the scientific community.

Acknowledgments

Dr. J.-P. Montillet, Dr. W. Finsterle, Dr. M. Haberreiter gratefully acknowledge the support from the Karbacher-Funds. Dr. J.-P. Montillet. also thanks the Swiss Space Office for support via the PRODEX funds supporting the making of the DARA dataset. Dr. D. Wu, Dr. X. Ye, Prof. P. Zhu, Dr. D. Yang, Prof. W. Fang, Dr. J. Qi and Dr. P.

Zhang acknowledge the National Nature Science Foundation of China (Grant Number 41974207) and CIOMP International Fund. This research is also supported by the International Space Science Institute (ISSI) in Bern, through ISSI International Team project No.500 (Towards Determining the Earth Energy Imbalance from Space). We also would like to acknowledge the help of Mr J. Vermeirssen in the development of this work.

Open Research

The composite *C3* can be obtained from the open archive repository *www.astromat.org* (Montillet et al., 2022, 2023). It is also presented on *www.pmodwrc.ch/en/?s = TSI+ Composite* (last accessed 30th October 2023) for additional information. The TSI composite *C1* is available for downloading at *http : //www.issibern.ch/teams/solarirradiance* (last accessed 05 November 2023). The composite *C6* is available at *https : //www.sidc.be/users/stevend/* (last accessed 30th October 2023). The data related to the monthly/daily mean sunspot numbers are retrieved from *http : //www.sidc.be/ silso/datafiles* (last accessed 30th October 2023). *TIM /SORCE*, TCTE/TIM and *TIM/TSIS* time series are downloaded from *https : //lasp.colorado.edu /home/sorce/data/tsi−data* (last accessed 30th October 2023). *PREMOS (v1)* can be accessed at *http : //idoc−picard.ias.u−psud.fr/sitools/client− user/Picard/project−index.html* (last accessed 30th October 2023). *PMODv21a* (also called *PMODv8*) is available at *https : //www.pmodwrc.ch/en/research−development/space/soho/* (last accessed 30th October 2023). The DARA 6-hourly product (JTSIM-DARAv1) is released either via the PMOD website (*https : //www.pmodwrc.ch/en/research−development/space/fy− 3e/* - see link to the ftp server) or via the open archive repository *www.astromat.org* (Montillet et al., 2023).

Appendix A Additional Figures

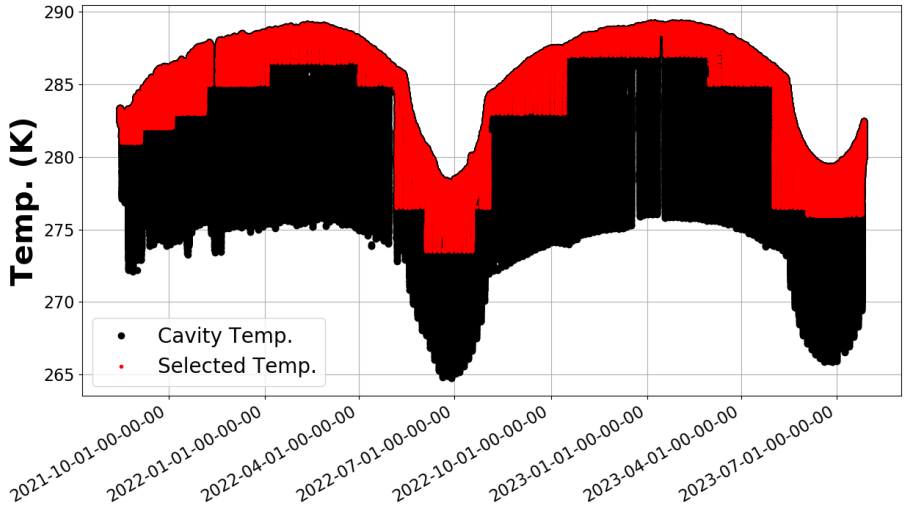

Figure A1: Cavity temperature in Kelvin (K) - filtered (red) and original (black)

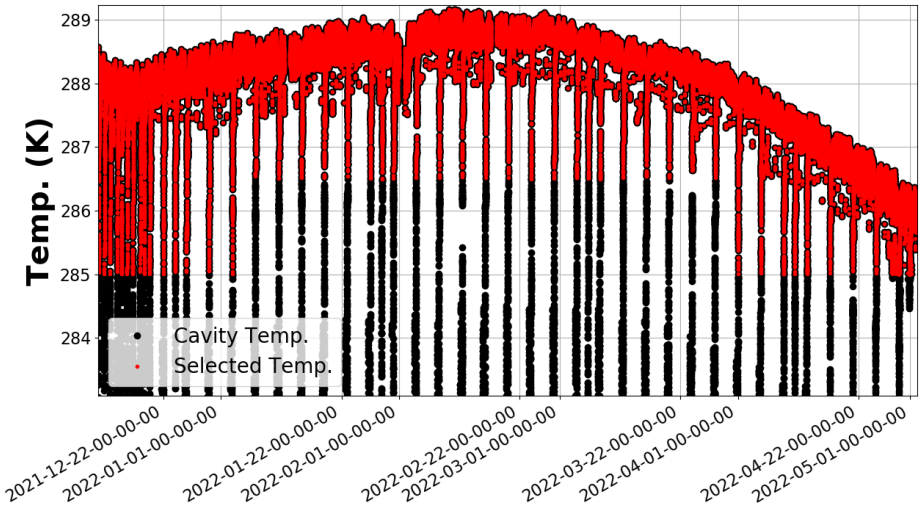

Figure A2: Cavity temperature in Kelvin (K) - filtered (red) and original (black) - zoom

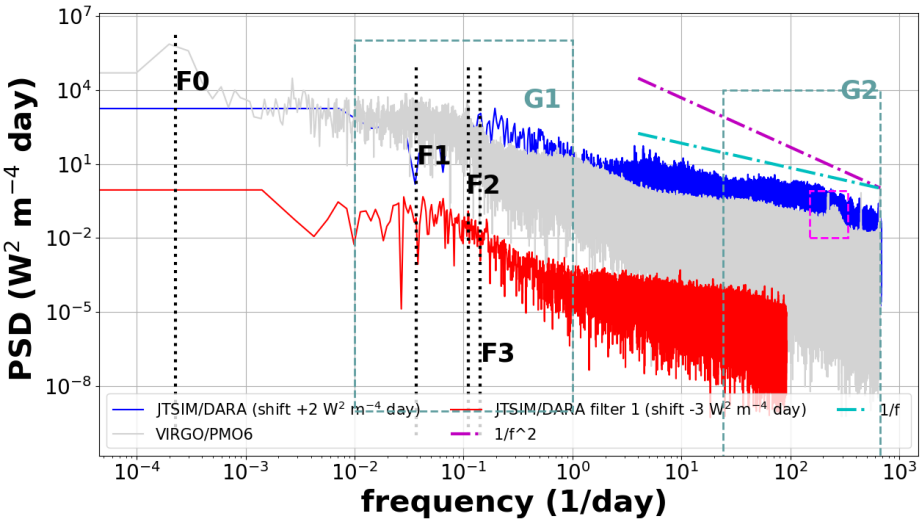

Figure A3: Power Spectrum Density analysis of the DARA 1 min rate TSI time series using the Welch's method applying filter 1 (red). The gray PSD is the 1 minute data rate of the observations recorded by the PMO6 radiometer on board of the SOHO/VIRGO mission. We emphasize the frequency band G1 at [1-100] days and the P-modes (dashed purple box). The black vertical dotted lines correspond to 11.5 years (F0), 27 days (F1), 9 days (F2) and 7 days (F3). The dashed line is the power-law model when varying the exponent (shown for context).

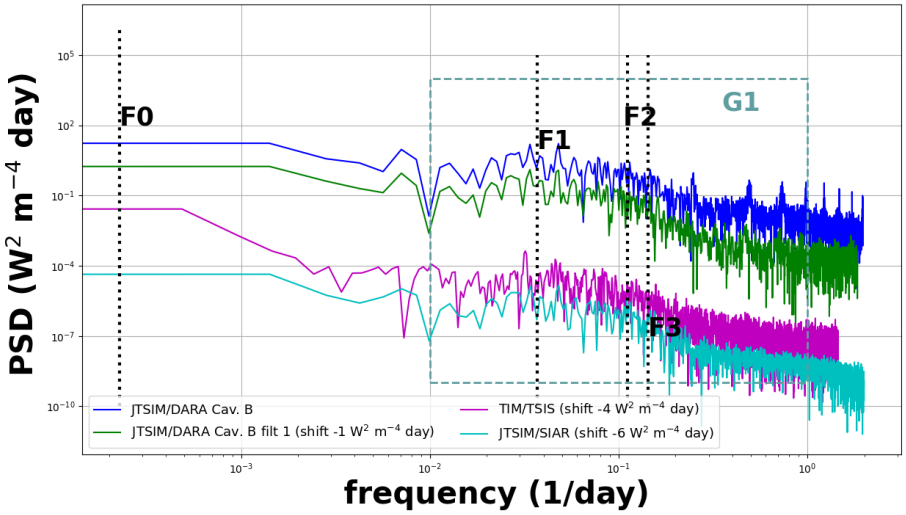

Figure A4: Power spectrum analysis of the DARA 6h rate TSI time series using the Welch's method applying filter 1. We also display the 6h data rate of the observations recorded by the VIRGO/PMO, SIAR and TSIS/TIM radiometers. The black vertical dotted lines correspond to 11.5 years (F0), 27 days (F1), 9 days (F2) and 7 days (F3).

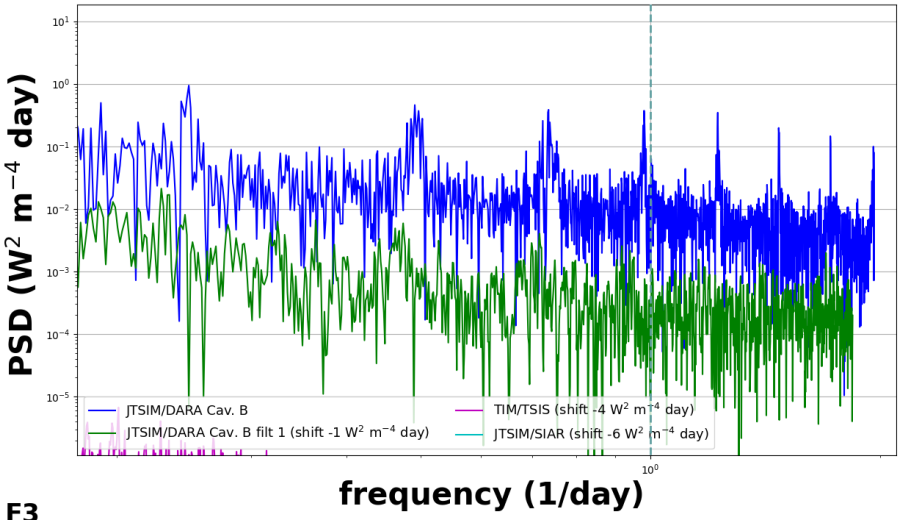

Figure A5: Power spectrum analysis of the DARA 6h rate TSI time series using the Welch's method applying filter 1 or not.

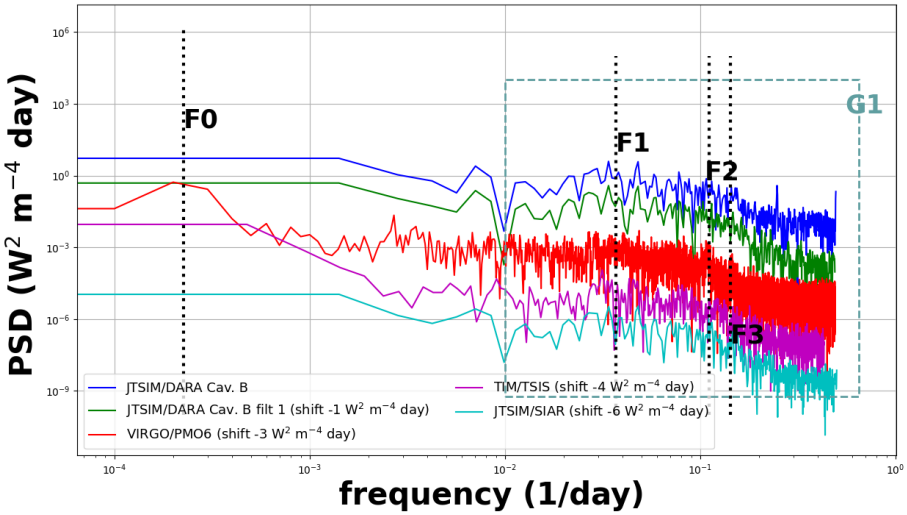

Figure A6: Power Spectrum Density of the DARA daily rate TSI time series using the Welch's method applying filter 1. We also display the daily data rate of the observations recorded by the VIRGO/PMO6, TIM/TSIS and SIAR radiometers. The black vertical dotted lines correspond to 11.5 years (F0), 27 days (F1), 9 days (F2) and 7 days (F3).

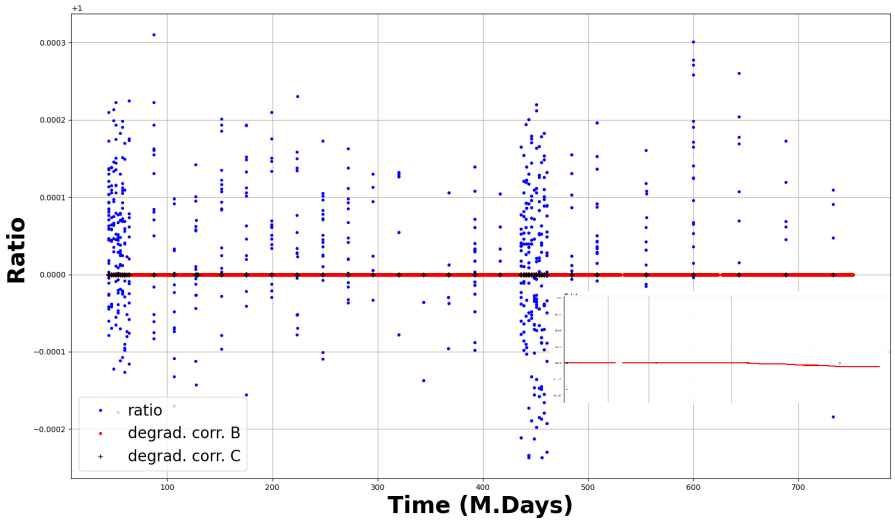

Figure A7: Ratio of the channels B and C as a function of the mission days. The red line is the degradation curve for the observations recorded by the cavity B. There is no degradation at this time for the back-up channel (black crosses). A zoom is also included showing a degradation of approximately 5 ppm.

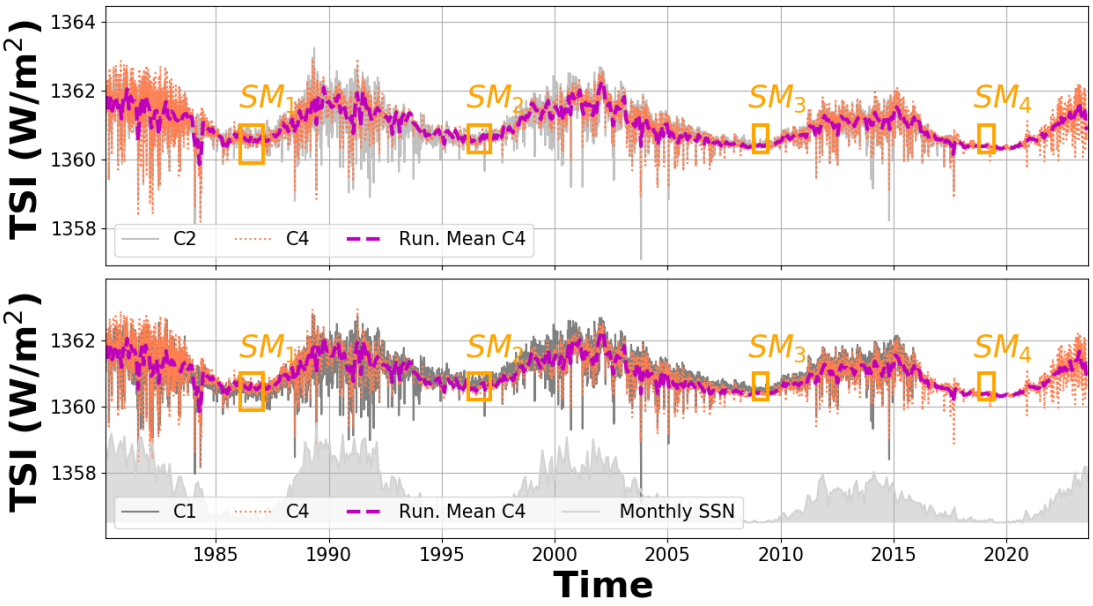

Figure A8: New composite (*C4*, orange) based on merging 43 years of TSI measurements. For comparison, *C2* (Fröhlich, 2006) and *C1* (Dudok de Wit et al., 2017) are also shown (grey line). A 30-day running mean of *C4* is shown as a yellow/purple dashed line. The orange boxes are associated with the solar minima (SM) for each solar cycle described in Table 3. For context, the monthly sunspot number is also displayed.

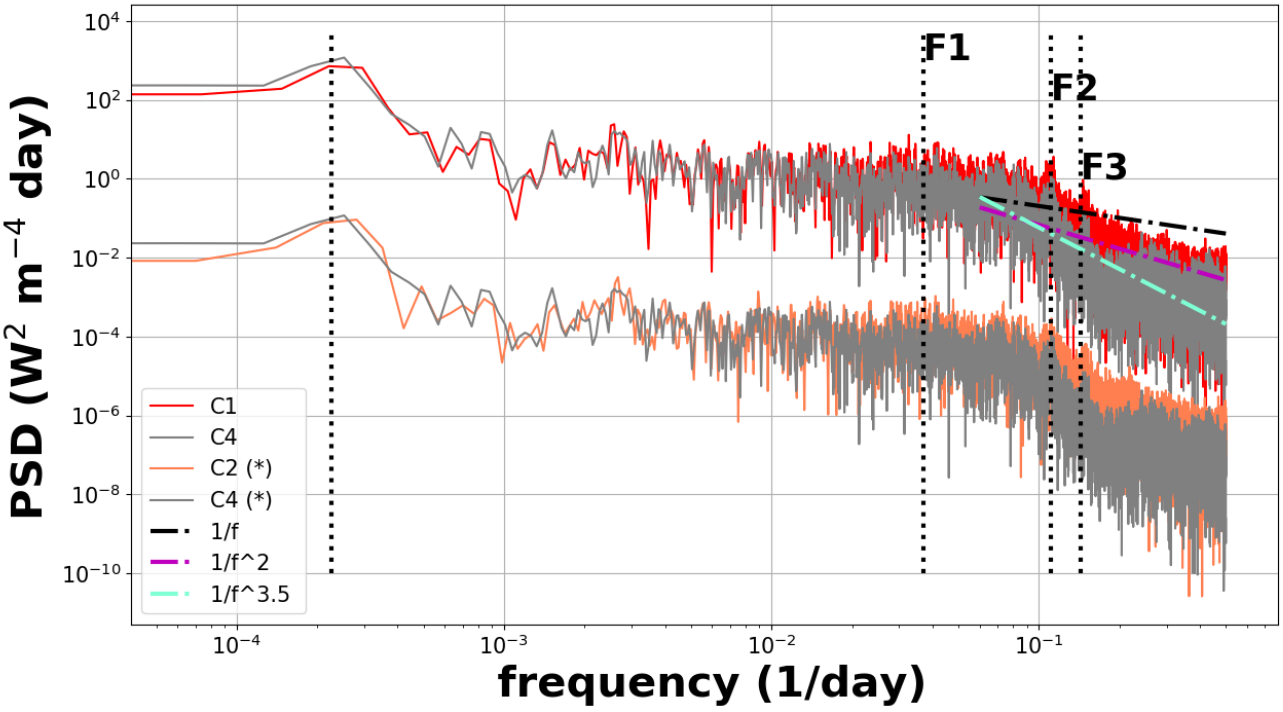

Figure A9: Power Spectrum Density of TSI *C1* (Dudok de Wit et al., 2017), *C2* (Fröhlich, 2006), together with the new TSI composite including the JTSIM-DARA product *C4* . The $(*)$ means that the time series are shifted by rescaling the amplitude by -4 W^2 m^{-4} day in the log-log plot. The dashed lines are the various power-law models when varying the exponent, which are only shown for context. The vertical doted lines (black) mark the frequencies at 27 (F1), 9 (F2) and 7 (F3) days.

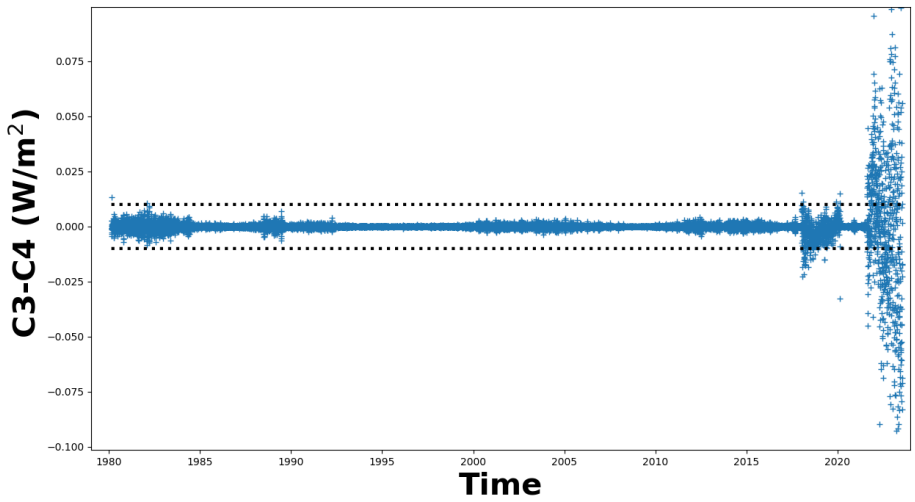

Figure A10: Difference between the TSI composite *C3* (Montillet et al., 2023) and the time series including the JTSIM-DARA product *C4*. The horizontal doted lines show the limit at 0.01 W/m^2.

References

Amdur, T., & Huybers, P. (2023). A bayesian model for inferring total solar irradiance from proxies and direct observations: Application to the acrim gap. *Journal of Geophysical Research: Atmospheres*, *128*(15), e2023JD038941. Retrieved from `https://agupubs.onlinelibrary.wiley.com/doi/abs/10.1029/2023JD038941` (e2023JD038941 2023JD038941) doi: https://doi.org/10.1029/2023JD038941

Andersen, B. N., Leifsen, T., & Toutain, T. (1994). Solar noise simulations in irradiance. *Sol. Phys.*, *152*, 247–252. doi: 10.1007/BF01473211

Ball, W. T., Schmutz, W., Fehlmann, A., Finsterle, W., & Walter, B. (2016). Assessing the beginning to end-of-mission sensitivity change of the PREcision MOnitor Sensor total solar irradiance radiometer (PREMOS/PICARD). *Journal of Space Weather and Space Climate*, *6*(27), A32. doi: 10.1051/swsc/2016026

Dewitte, S., Cornelis, J., & Meftah, M. (2022). Centennial total solar irradiance variation. *Remote Sensing*, *14*(5). Retrieved from `https://www.mdpi.com/2072-4292/14/5/1072` doi: 10.3390/rs14051072

Dewitte, S., & Nevens, S. (2016). The Total Solar Irradiance Climate Data Record. *The Astrophysical Journal*, *830*(1), 25. doi: 10.3847/0004-637x/830/1/25

Dudok de Wit, T., & Kopp, G. (2020). *1/f noise in irradiance records affects our understanding of trends in solar radiative forcing.* (AGU conference, A237-08)

Dudok de Wit, T., Kopp, G., Fröhlich, C., & Schöll, M. (2017). Methodology to create a new total solar irradiance record: Making a composite out of multiple data records. *Geophys. Res. Lett.*, *44*, 1196–1203. doi: 10.1002/2016GL071866

Finsterle, W., Montillet, J., Schmutz, W., Sikonja, R., Kolar, L., & Treven, L. (2021). The total solar irradiance during the recent solar minimum period measured by SOHO/VIRGO. *Scientific Reports*, *11*(7835), 10. doi: 10.1038/s41598-021-87108-y

Fröhlich, C. (2003). Long-term Behaviour of Space Radiometers. *Metrologia*, *40*, 560–565. doi: 10.1088/0026-1394/40/1/314

Fröhlich, C. (2006). Solar Irradiance Variability Since 1978. Revision of the PMOD Composite during Solar Cycle 21. *Space Science Reviews*, *125*, 53–65. doi: 10.1007/s11214-006-9046-5

Fröhlich, C., Andersen, B., & Appourchaux, T. e. a. (1997). First Results from VIRGO, the Experiment for Helioseismology and Solar Irradiance monitoring on SOHO. *Solar Physics*, *170*, 1–25. doi: 10.1023/A:1004969622753

Fröhlich, C. (2006). Solar irradiance variability since 1978. *Space Sci. Rev.*, *125*, 53–65. doi: 10.1007/s1121400690465

Fröhlich, C., & Lean, J. (2004). Solar radiative output and its variability: Evidence and mechanisms. *Astron. Astrophys. Rev.*, *12*, 273—320. doi: 10.1007/s00159-004-0024-1

Kopp, G., Lawrence, G., & Rottman, G. (2005). The Total Irradiance Monitor (TIM): Science Results. *Sol. Phys.*, *230*(1-2), 129-139. doi: 10.1007/s11207-005-7433-9

Kopp, G., & Lean, J. L. (2011). A new, lower value of total solar irradiance: Evidence and climate significance. *Geophys. Res. Lett.*, *38*, L01706. doi: 10.1029/2010GL045777

Mekaoui, S., & Dewitte, S. (2008). Total solar irradiance measurement and modelling during cycle 23. *Sol. Phys.*, *247*, 203–216. doi: 10.1007/s11207-007-9070-y

Montillet, J., Finsterle, W., Koller, S., Pfiffner, D., & Gyo, M. (2023). *Total solar irradiance recorded by the fy3e/dara-jtsim radiometer, version 1.0.* `https://doi.org/10.60520/IEDA/113059`. Interdisciplinary Earth Data Alliance (IEDA). (Accessed 2023-11-11)

Montillet, J., Finsterle, W., Schmutz, W., Haberreiter, M., Dudok de Wit, T., Kermarrec, G., & Sikonja, R. (2022). [dataset]. composite pmod data fusion. *Interdisciplinary Earth Data Alliance (IEDA), https:/doi.org/10.26022/IEDA/112238, Accessed 2022-06-07*.

Montillet, J., Finsterle, W., Schmutz, W., Haberreiter, M., Dudok de Wit, T., Kermarrec, G., & Sikonja, R. (2023). [dataset]. composite pmod data fusion. *Interdisciplinary Earth Data Alliance (IEDA), https://doi.org/10.26022/IEDA/112940, Accessed 2023-06-01*.

Montillet, J.-P., Finsterle, W., Haberreiter, M., Schmutz, W., & et al. (2022). Solar Irradiance monitored by DARA/JTSIM : first light observations. In *Egu general assembly* (Vol. EGU22-616). doi: 10.5194/egusphere-egu22-616

Montillet, J.-P., Finsterle, W., Kermarrec, G., Sikonja, R., Haberreiter, M., Schmutz, W., & Dudok de Wit, T. (2022). Data fusion of total solar irradiance composite time series using 41 years of satellite measurements. *Journal of Geophysical Research: Atmospheres*, *127*(13), e2021JD036146. Retrieved from `https://agupubs.onlinelibrary.wiley.com/doi/abs/10.1029/2021JD036146` (e2021JD036146 2021JD036146) doi: https://doi.org/10.1029/2021JD036146

Qi, J., Zhang, P., Qiu, H., Fang, W., Ye, X., & Yu, P. (2015). Analysis of total solar irradiance observed by fy-3c solar irradiance monitor-ii. *Chinese Science Bulletin*, *60*, 2447-2454. Retrieved from `https://doi.org/10.1360/N972015-00471` doi: 10.1360/N972015-00471

Remesal Oliva, A. (2021). *Understanding and improving the cavity absorptance for space TSI radiometers* (Unpublished doctoral dissertation). University of Zurich.

Scafetta, N., & Willson, R. C. (2019). Comparison of decadal trends among total solar irradiance composites of satellite observations. *Advances in Astronomy*, *2019*. Retrieved from `https://doi.org/10.1155/2019/1214896` doi: 10.1155/2019/1214896

Schmutz, W., Fehlmann, A., Finsterle, W., Kopp, G., & Thuillier, G. (2013). Total solar irradiance measurements with PREMOS/PICARD. In *American institute of physics conference series* (Vol. 1531, pp. 624–627). doi: 10.1063/1.4804847

Schmutz, W. K. (2021). Changes in the total solar irradiance and climatic effects. *J. Space Weather Space Clim.*, *11*, 40. Retrieved from `https://doi.org/10.1051/swsc/2021016` doi: 10.1051/swsc/2021016

Shapiro, A., Solanki, S., Krivova, N., Cameron, R., Yeo, K., & Schmutz, W. (2017). The nature of solar brightness variations. *Nat. Astron.*, *1*, 612–616. doi: 10.1038/s41550-017-0217-y

Song, B., Ye, X., Finsterle, W., Gyro, M., Gander, M., Oliva, A. R., ... Fang, W. (2021). The Fengyun-3E/Joint Total Solar Irradiance Absolute Radiometer: Instrument Design, Characterization, and Calibration. *Solar Physics*, *296*(3). doi: 10.1007/s11207-021-01794-5

Thuillier, G., Dewitte, S., Schmutz, W., & Picard Team. (2006). Simultaneous measurement of the total solar irradiance and solar diameter by the PICARD mission. *Advances in Space Research*, *38*, 1792–1806. doi: 10.1016/j.asr.2006.04.034

von Savigny, C., Peters, D. H. W., & Entzian, G. (2019). Solar 27-day signatures in standard phase height measurements above central Europe. *Atmos. Chem. Phys.*, *19*. doi: 10.5194/acp-19-2079-2019

Walter, B., Andersen, B., Beattie, A., Finsterle, W., Kopp, G., Pfiffner, D., & Schmutz, W. (2020). First TSI results and status report of the CLARA/NorSat-1 solar absolute radiometer. In M. T. Lago (Ed.), *Astronomy in focus* (Vol. 14). Cambridge University Press. doi: 10.1017/S1743921319004617

Wang, Y., Fang, W., Gong, C., & Yu, B. (2007). Dual cavity inter-compensating absolute radiometer. *Opt. Precis. Eng.*, *15*(1662). doi: 10.3321/j.issn:1004-924x

.2007.11.005

Wilson, R. (1997). Total solar irradiance trend during solar cycles 21 and 22. *Science*, *277*, 1963–1965. doi: 10.1126/science.277.5334.1963

Wilson, R. (2014). ACRIM3 and the Total Solar Irradiance database. *Astrophys Space Sci.*, *352*, 341–352. doi: 10.1007/s10509-014-1961-4

Yeo, K. L., Krivova, N. A., & Solanki, S. K. (2014). Solar cycle variation in solar irradiance. *Space Science Reviews*, *136*, 137-167. Retrieved from `https://doi.org/10.1007/s11214-014-0061-7` doi: 10.1007/s11214-014-0061-7

Young, A. C., Cortés, R., Caussade, A., & Maimone, M. (2023). *Sun activity archive.* `https://earthsky.org/sun/sun-activity-archive-for-april-2023/`. (Accessed: (01.12.2023))

Zhu, P., Ye, X., Montillet, J.-P., Finsterle, W., Yang, D., Duo, W., ... Zhang, P. (2023). The first light from the joint total solar irradiance measurement experiment onboard the FY3-E meteorological satellite. *Earth and Space Science*, *0*(0). doi: 0